Journal Name

ARTICLE

Tuning Plasmons Layer-by-Layer for Quantitative Colloidal Sensing with Surface-enhanced Raman Spectroscopy

Received 00th January 20xx,
Accepted 00th January 20xx

DOI: 10.1039/x0xx00000x

William J. Anderson[a], Kamila Nowinska[a], Tanya Hutter[b], Sumeet Mahajan[a]* and Martin Fischlechner[a]*

Surface-enhanced Raman spectroscopy (SERS) is well known for its high sensitivity that emerges due to the plasmonic enhancement of electric fields typically on gold and silver nanostructures. However, difficulties associated with the preparation of nanostructured substrates with uniform and reproducible features limits reliability and quantitation using SERS measurements. In this work we use layer-by-layer (LbL) self-assembly to incorporate multiple functional building blocks of collaborative assemblies of nanoparticles on colloidal sphere to fabricate SERS sensors. Gold nanoparticles (AuNPs) are packaged in discrete layers, effectively 'freezing nano-gaps', on spherical colloidal cores to achieve multifunctinality and reproducible sensing. Coupling between layers tunes the plasmon resonance for optimum SERS signal generation to achieve a 10 nM limit of detection. Significantly, using the layer-by-layer construction, SERS-active AuNP layers are spaced out and thus optically isolated. This uniquely allows the creation of an internal standard within each colloidal sensor to enable highly reproducible self-calibrated sensing. By using 4-mercaptobenzoic acid (4-MBA) as the internal standard adenine concentrations are quantified to an accuracy of 92.6-99.5%. Our versatile approach paves the way for rationally designed yet quantitative colloidal SERS sensors and their use in a variety of sensing applications.

Introduction

Surface-enhanced Raman spectroscopy (SERS) uses the amplification of Raman scattering by a chemical (CM) enhancment mechanism along with, a usually more pronounced, electromagnetic (EM) enhancment mechanism on nano-structured coinage materials (typically gold and silver)[1–3] which can result in the detection of even single-molecules.[4,5] Enhancements are highly dependent on the localized surface plasmon resonance (LSPR) of the nanomaterials.[6,7] However, to deliver reproducible enhancements, strict control over material nanostructuring or ensemble averaging approaches is required. Various nanostructuring methods such as electron beam lithography,[8] nanoimprint lithography,[9] nanosphere lithography[10] and electrochemical deposition[11] have been used. These techniques are typically applied to planar substrates and, despite the complexity of these methods, precise control at the 1–10 nm SERS length scales remains elusive. In contrast, colloidal SERS offers a relatively simple approach with several advantages over planar substrates, including reduced sample volumes and large surface areas. The latter allowing for ensemble averaging in small volumes.[12]

Colloidal SERS is commonly performed by aggregating (*e.g.* by adding salts) nanoparticles with analytes; the aggregation results in plasmon 'hot spots' to deliver high enhancements. This popular approach does not allow spatio-temporal control, resulting in polydisperse aggregates and thus low measurement reproducibility.[13] Use of spacer molecules to control the nanogap between colloidal nanoparticles has been used to control and improve reproducibility of aggregation.[14] However, lack of temporal control and potential interference from analytes or other aggregation-agents in solution makes the approach less generic. Microfluidics has also been employed for reproducible homogenisation of the nanoparticle-analyte-aggregating agent mixture to improve monodispersity,[15–17] but such approaches introduce experimental complexity and difficulties. Alternatively pre-aggregated NPs can be straightforwardly trapped within a polymer film with highly uniform plasmonic properties (3.2% deviation).[18] While simple, the approach is unsuitable for the inclusion of multiple functional elements with defined nanoscopic control, thereby limiting the functional sophistication of the SERS sensor.

A promising alternative for the construction of SERS-substrates is to 'freeze' plasmonic nanogaps by mounting nanoparticles on planar or colloidal substrates using a layer-by-layer (LbL) self-assembly strategy. LbL fabrication is a powerful approach that enables the construction of polyelectrolyte-based composite materials through iterative cycles of adsorption.[19–21] Its sequential nature allows the incorporation of a multitude of charged functional building blocks within and across layers in tightly controlled arrangements.[20,22–24] Feasibility of using LbL self-assembly for SERS substrate construction has been shown on planar substrates[25–28] and extended to coating silver nanoparticles on a silica microsphere.[29] However, neither the versatility offered by LbL technology nor the

[a] *Department of Chemistry and Institute for Life Sciences, University of Southampton, Highfield, SO17 1BJ, United Kingdom.*
[b] *Department of Chemistry, University of Cambridge, Lensfield Road, Cambridge CB2 1EW, United Kingdom*

Electronic Supplementary Information (ESI) available: [Materials and methods, Various scattering spectra, simulation results, SERS intensity scatter plots, enhancement factor calculation, Table of SERS performance of sensors, Representative raw SERS spectra and control Raman and SERS spectra of MBA and sensors (FigS1-8)]. See DOI: 10.1039/x0xx00000x

ability to create tuneable and programmable sensor architectures has been demonstrated for highly sensitive and yet reproducible and quantitative sensing. Achieving high sensitivity along with reproducibility and quantitation is a much vaunted goal in molecular sensing which we address here.

In this work, we demonstrate the advanced versatility of the LbL approach to fabricate plasmon-tuneable, sensitive, quantitative and self-calibrating colloidal SERS sensors. Using alternate coatings of gold nanoparticles (AuNPs) and polyelectrolyte 'spacer' layers to control nanoparticle spacing in the radial direction, it is shown that plasmonic coupling can be tuned to specific LSPRs. Sequential LbL deposition additionally allows the creation of independent SERS-active layers to accommodate internal standards for calibrated quantitative measurements. AuNPs are adsorbed directly from their colloidal suspension without addition of any further salt. Consequently AuNP assembly creates uniform deposition at the layer of choice without polydisperse aggregates, overall enabling the controlled fabrication of reproducible AuNP sensors. Thus our versatile approach of creating 3D plasmonic architectures using the LbL method on microspheres combines the advantages of colloidal sensors and ensemble averaging to yield sensitive yet reproducible and quantitative sensors.

Experimental

Materials

Polystyrene microparticles (19.5 μM, 10% (v/v) in aqueous suspension) were purchased from Microparticles GmbH. Citrate-capped AuNPs (40 nm, 8% CV, 9 x 10^{10} particles ml^{-1}) were purchased from BBI Solutions. Poly(ethyleneimine) (PEI) (M_w ~750 000 g/M, 50% (wt) in water) and poly(sodium 4-styrenesulfonate) (PSS) (M_w ~70 000 g/M) were purchased from Sigma-Aldrich and diluted to 2 mg/mL in 0.5 M NaCl. Polyelectrolyte solutions were sterile filtered (0.22 μM pore size) after preparation. 4-mercaptobenzoic acid (4-MBA) (99%) and adenine (≥99%) were purchased from Sigma-Aldrich. 4-MBA was diluted to 1 mM in ethanol, with further dilution in acetate buffer (100 mM, pH 5) prior to use. Adenine was diluted to 1 mM in Milli-Q water and diluted further in acetate buffer (100 mM, pH 5).

Sensor Fabrication

The initial PEI/PSS/PEI polyelectrolyte cushion was adsorbed by pipetting polystyrene microparticles (typically 50 μl of 10% v/v) into an Eppendorf filled with polyelectrolyte solution (2mg/mL, 0.5M NaCl, typically 400 μl) followed by shaking for 20 minutes. The particles were washed three times in water by centrifugation. AuNP-layers were applied by pipetting beads into an Eppendorf filled with AuNPs (used as provided by BBI Solutions) followed by shaking for one hour. The amount of nanoparticles was calculated as such, that excess concentrations were used (2x coverage of the entire surface area). After incubation the beads were washed by centrifugation (1400 g, 90 seconds) until the supernatant was clear. Further layers of polyelectrolyte and AuNPs were applied as described above. Sensors were stored at 4 °C in acetate buffer (pH 5) until use (typically within 1 week).

Sensor Application

Sensors were exposed to analyte by pipetting 5 μL of 0.1% (v/v) microparticles into 20 μL of analyte following shaking for 30 minutes at room temperature. The sample was then washed 3x in acetate buffer to remove any non-adsorbed molecules. Measurements were made on the same day.

TEM

Sensors were washed and suspended in 500 μL of Milli-Q water and 1% (w/v) sodium alginate (Sigma-Aldrich). The samples were then centrifuged to form a pellet prior to addition of 0.1 M $CaCl_2$ for gelation. An ethanol series was used to dehydrate the pellets, followed by 3 washes and soaks in Spurr resin (Sigma-Aldrich). The resin was heated to 60°C for 24 hours until cured. 120 nm sections (obtained using a Reichert Ultracut E ultramicrotome with glass knife) were applied to copper TEM grids and imaged.

Instrumentation

Static light scattering measurements were performed with an OceanOptics DH-2000 UV-Vis-NIR source and an OceanOptics USB2000 spectrometer. The incident white light was collimated and scattering spectra were collected orthogonal to incident radiation (Figure M1, see ESI). The scattering intensities were normalised using a diffuser to correct for system spectral variation in the source as well as the detector. Bright-field images were acquired using a Nikon Eclipse LV100 microscope (20x objective with 0.45 N.A.). TEM images were acquired using an FEI Tecnai T12 Transmission Electron Microscope (87000x magnification). The Raman measurements were performed on a Renishaw InVia spectrometer. Both 633 nm (He-Ne laser, 6 mW max output) and 785 nm (solid-state diode laser, 120 mW max output) excitation sources were used. The power output was adjusted to approximately 0.25 mW - 0.5 mW at the objective (Olympus, 0.40 N.A., 20x) and measured prior to each experiment. Sensors were measured individually with 10 second extended scans. Processing was performed with IRootLab[30] and Renishaw's WiRE software.

Simulations

Finite-element simulations were performed using COMSOL Multiphysics v5.3, with Wave Optics Module. A three-dimensional model of an array of gold nanoparticles with radius of 20 nm and varying gap between the particles was constructed. The surrounding medium sphere radius was 800 nm surrounded by Perfectly Matched Layer (PML) of 200 nm thickness to act as an absorber of the scattered field to eliminate back reflections. A plane wave was travelling at a positive x direction with electric field polarisation along the z-axis. Refractive index of water was taken as 1.33, and of gold was taken from COMSOL Optical Materials Database. Wavelength range was between 400 and 900 nm with a step size of 10 nm. Figure M2 (see ESI) demonstrates the geometry of the simulation model and the equations used.

Results and Discussion

Fabrication of sensors

Figure 1 illustrates the key steps involved in fabricating the sensors. First an initial polyelectrolyte cushion consisting of at least three polyelectrolyte layers (poly(ethyleneimine) (PEI)/ poly(sodium 4-styrenesulfonate) (PSS)/PEI, with PEI being cationic and PSS being anionic; alternate layers deposit due to electrostatic attraction between oppositely charged species) is applied to 20-µm-diameter polystyrene beads to provide a reproducible foundation for further modifications independent of the template material (the bead used as core).[19] Alternating layers of negatively charged AuNPs and the cationic polyelectrolyte PEI are then applied. While adsorption of PEI layers is conducted in 0.5M NaCl solution to ensure that the polyelectrolyte is fully soluble (in the fluid phase)[31] enabling rapid and complete layer assembly, the nanoparticles are adsorbed directly from their colloidal suspension to prevent aggregation.

In order to minimise AuNP consumption, 20 µm beads were used as a template. This enables a larger volume of microparticles (1-5% v/v) to be used whilst limiting AuNP concentrations required for coating in this study. However, essentially any material can be used as a template or a coating layer, providing it carries an appropriate charge and posesses suitable dimensions.[32] Furthermore, the size of the core, 1 – 20 µm diameter was not found to have any effect on the optical properties resulting from LbL deposition of AuNP layers (see Figure S1 in ESI).

By introducing AuNPs in a sequential layer-by-layer fashion, it is possible to design SERS sensing elements in a highly defined manner. Figure 2 shows samples coated with one to four layers of AuNPs, connected via single coatings of the polycation PEI. The sensors are illustrated in Figure 2a, with corresponding bright-field images in Figure 2b. Sensors with one single AuNP layer appear red, demonstrating that the majority of the coating consists of an AuNP sheet (*i.e.* non-aggregated). Additional AuNP layers shift the colour towards dark blue and purple, indicating that strong plasmon coupling occurs across layers. Figure 2c documents TEM images of microtomed sensor sections with one and four AuNP layers. A single coating of AuNPs (Ø40 nm; CV8%) results in a layer with an average thickness of 40–60 nm, in essence attaining a monolayer coating. Although the TEM images are obtained after several processing steps even involving dehydration (see experimental section) it is clear that 4 AuNP coatings yield a total thickness of 160–200 nm.

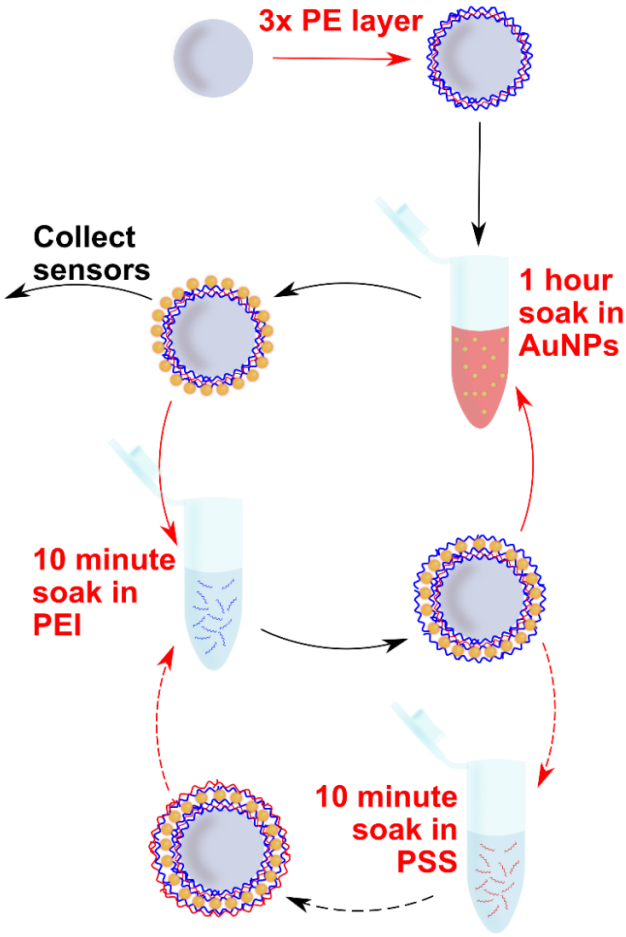

Figure 1: Fabrication of colloidal SERS sensors. An initial polyelectrolyte cushion where a blue layer is PEI (cationic) and a red layer is PSS (anionic) is applied to polystyrene microspheres to provide uniformly charged surfaces. Alternate AuNP (gold sphere) is applied to polystyrene microspheres to provide uniformly charged surfaces. Alternate AuNP and polyelectrolyte layers (to space out to control and/or isolate) are then applied to fabricate SERS active or inactive regions by iterative cycles of incubation and washing by centrifugation.

This indicates that adsorbing PEI/AuNP layer pairs follow a linear, monolayer by monolayer assembly sequence. While due to the complex processing steps involving dehydration the precise spacing between AuNPs with a layer and between the layers could not be determined by TEM, the systematic tuneability of plasmon resonances backed up by our simulation results provide insight into the spacing of AuNPs. This is discussed in the next section.

Tuneability of plasmon resonances

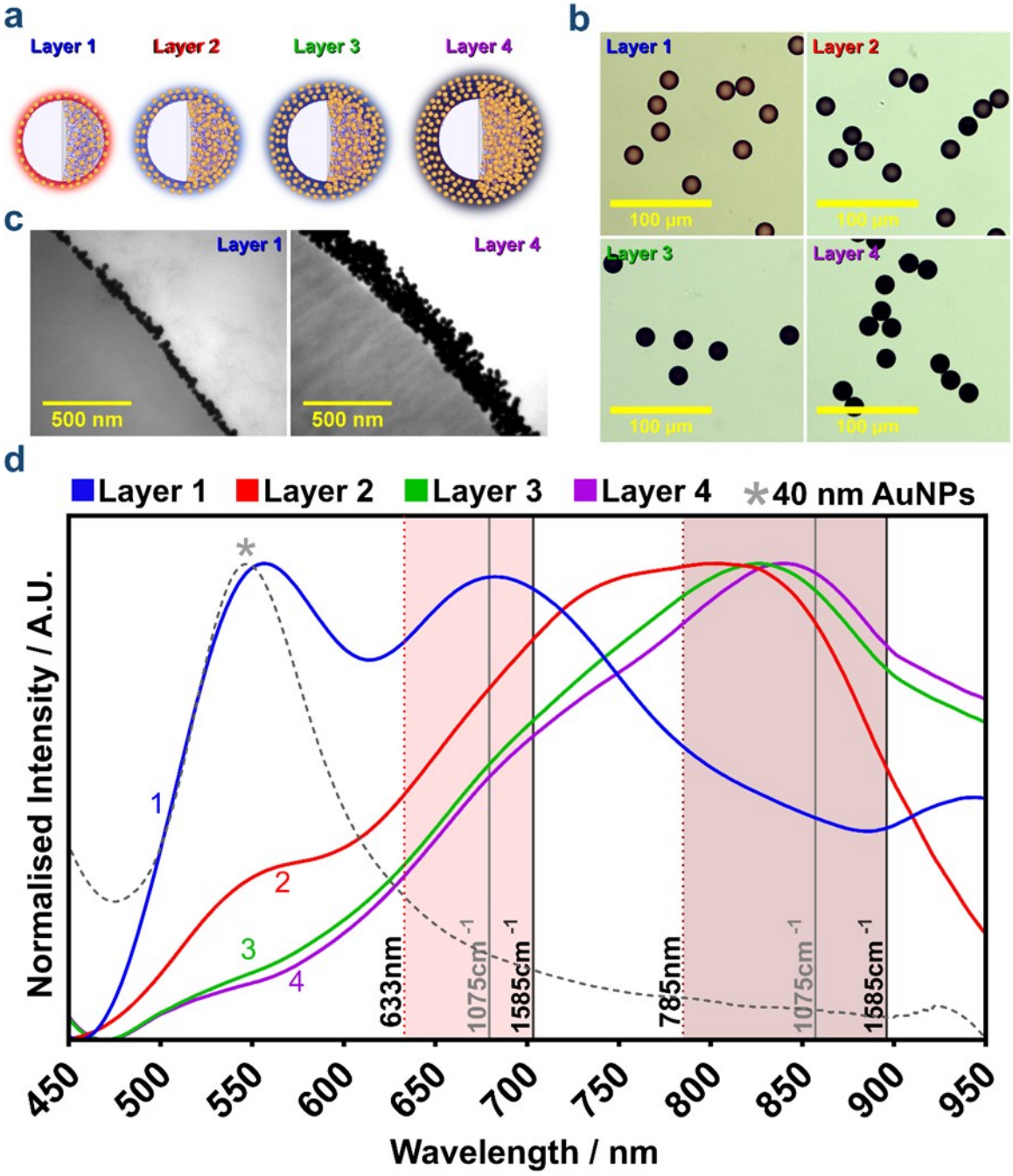

Figure 2:(a) Schematic representation of sensors decorated with one to four AuNP layers. (b) Associated bright-field images of coated 20-µm-diameter polystyrene beads. The shift from red to the deep blue colour with increasing AuNP layers indicates that nanoparticle coupling mainly occurs across layers. (c) TEM images of beads coated with one and four PEI/AuNP layer pairs (PEI stains were not used). (d) Normalised scattering data of the different samples and scattering of single 40 nm AuNPs (dashed line). A single AuNP layer (blue) reveals a LSPR signature correlating to a mixture of predominantly single 40 nm AuNPs. The addition of further layers results in a pronounced LSPR shift towards higher wavelengths, showing that AuNP-coupling occurs across layers. The 1075 cm^{-1} and 1585 cm^{-1} peak emission wavelengths are indicated for 4-mercaptobenzoic acid (4-MBA) used as the SERS reporter molecule with 633 and 785 nm excitations.

The scattering spectra of the colloidal sensors plotted in Figure 2d show the evolution of plasmon resonances with sequential LbL coatings of nanoparticles. For sensors with a single layer of AuNPs, there are two main LSPR peaks, one at 550 nm and a second emerging at approx 680 nm. The former predominantly represents singular AuNPs, and the latter coupled AuNPs within the layer. Single nanoparticle spectra in water shows a scattering peak at 545 nm as expected (dotted spectrum in Fig. 2d). The slight shift to 550 nm in sensors could be expected due to the slightly different dielectric environment with the polyelectrolyte layers and the polystyrene bead. Scattering intensity is proportional to the squared volume,[33] thus larger assemblies of AuNPs will have a higher contribution. Therefore the spectrum of the sensor with a single layer indicates that the majority of AuNPs remain in an uncoupled state. However, the peak at ~680 nm is due to coupling between AuNPs within the layer which at smaller separations shows

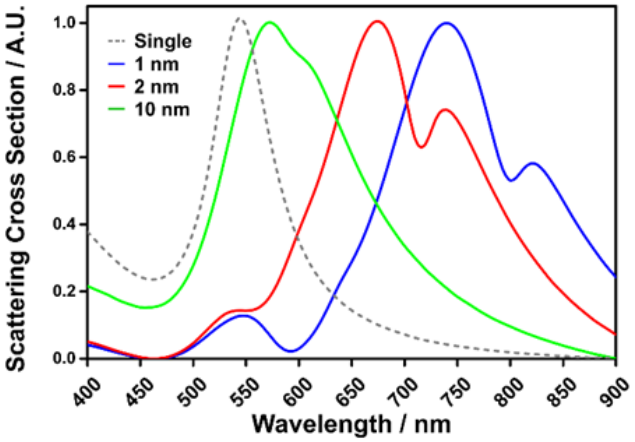

Figure 3. Simulations to show effect of spacing between nanoparticles within a single-layer array. Finite-element simulations were performed using COMSOL Multiphysics v5.3. An array of 5x5 nanoparticles (40 nm diameter) in water was used. The array was oriented 45° to the incident optical field to mimic the situation on sensors where multiple polarisations would interact with the layered nanoparticles on the colloid surface. The gap between the nanoparticles is varied here and the resulting normalised scattering cross-section spectra are shown. A simulated single nanoparticle spectrum (dotted line) is shown for comparison. The simulated single nanoparticle spectrum agrees completely with the experimentally observed scattering spectrum of nanoparticles (singular/unaggregated) in a colloidal solution.

the well-known red-shift in the dipolar plasmon resonance. This observation is consistent with simulations carried out with a planar array of gold nanoparticles at different spacings (Figure 3). It can be seen that the red-shifted Fano-like resonances arise due to plasmon coupling.[34] Relevant to this work it is important to note that with a decrease in interparticle spacing the plasmon modes red-shift. In fact using our simulation results it can be postulated that within the first layer the spacing between nanoparticles is inhomogenous but likely not smaller than 2 nm since the simulated spectrum for a 2 nm gap shows a red-shifted peak also around 680 nm which agrees well with the 2nd peak in the measured spectrum of sensors with 1-layer of AuNPs. The peak at 550 nm markedly reduces with the 2nd layer confirming that the uncoupled nanoparticles in the first layer have been plasmonically coupled. This could be by filling of the gaps remaining after the deposition of the first layer and additionally by deposition of a 2nd layer of nanoparticles. Since only a single polyelectrolyte spacer layer is used it would be expected that the coupling in the radial direction (vertical direction to the plane of AuNP layer) would be strong given that the separation would not be expected to be more than 1-2 nm. This coupling also would result in a red-shift of the dipolar (and multipolar) plasmon resonances consistent with increased plasmonic coupling[35–37] as the number of interacting particles in the radial direction increases with addition of sequential layers. The heterogeneity in separations as expected in AuNP coating layers in a solution-based LbL appraoch therefore leads to the broad peak observed between 700 and 850 nm to red-shift further on addition of subequent 3rd and 4th layers. The multiplicity of spectral features is also expected due to multiple orientations (polarisations) on the sensor giving rise to ensemble-averaging in the experimentally observed spectra. Nevertheless, the trend that multipolar plasmon peaks will red-shift on vertical coupling between layers is supported by our simulations of 2-layer arrays that are compared to 1-layer arrays (Figure S2). Spectral features in the scattering spectra obtained by simulations show broadening (due to increase in number of multipolar peaks) and a red-shift of all spectral features as the spacing reduces both within a layer and between the layers. From a comparison it can be seen that our experimentally observed scattering spectra are most similar to the case of Fig. S2d wherein both the spacing between AuNPs within a layer and between the layers is 2 nm.

SERS sensor characterisation

Being able to tune the LSPR is an exciting prospect for SERS sensor design; the electro-magnetic enhancement for SERS is an E^4 approximation, with E^4 being derived from a product of E^2 for the incident photons and E^2 for the scattered photons,[3,38] where E is the electric field. Therefore it is critical that the surface plasmon is not only in resonance with the incident wavelength but also with the wavelength of the scattered photons; this is especially relevant with red and NIR excitations as the Raman scattered wavelengths can differ remarkably. The layer-by-layer approach allows tuning of the LSPR sensors within a wide range, enabling the optimization towards a specific excitation wavelength, and enhancing their detection sensitivity to the major peaks of a given analyte.

To illustrate the approach we chose 4-mercaptobenzoic acid (4-MBA) as a SERS reporter molecule due to its high binding affinity with AuNPs via a thiol group and the presence of two distinct ring-breathing vibrational modes at 1075 cm^{-1} and 1585 cm^{-1}.[39] The scattering data indicates that plasmon resonances would be better suited for a 633 nm excitation with single layer sensors than with a 785 nm excitation (see Figure 2d). In contrast, for sensors with two to four AuNP layers, the 785 nm excitation should be better suited. To verify this hypothesis, the different sensor configurations were tested for their SERS signals. The sensors were first exposed to 10 μM 4-MBA solution for 30 minutes and retrieved by centrifugation to discard unbound molecules before SERS measurements were made. Spectra were taken from 10 individual sensors from each of the 1-4 layer samples.

The measured SERS spectra shown in Figure 4a (with corresponding peak intensities in Figure 4c; intensities from each sensor are shown as a scatter plot in Figure S3a) with 633 nm excitation reveal that all sensors show a distinct signal for the two ring-breathing peaks of 4-MBA (raw spectra and controls are presented in supporting information at Fig. S7 and Fig. S8). While the single layer sensors show a clear spectrum, the addition of a second AuNP layer increases the signals. However, the addition of subsequent layers diminishes the observed SERS intensities at this excitation wavelength. It is possible that the addition of a second layer results in a net increase in actual short-range plasmonic interactions as the gaps on the surface are filled replacing the long-range coupling. Another contribution to the signal will be the increased amount of gold surface available for attachment of analyte in saturating conditions. However, subsequent additional AuNP layers on the sensors results in de-tuning of the plasmonic resonances that are excited by the 633 nm excitation, thus significantly reducing SERS enhancements. On the other hand with 785 nm excitation (Figure 4b, d ; intensities from each sensor are shown as a scatter plot in Figure S3b), the single AuNP layer sensor produces weak SERS

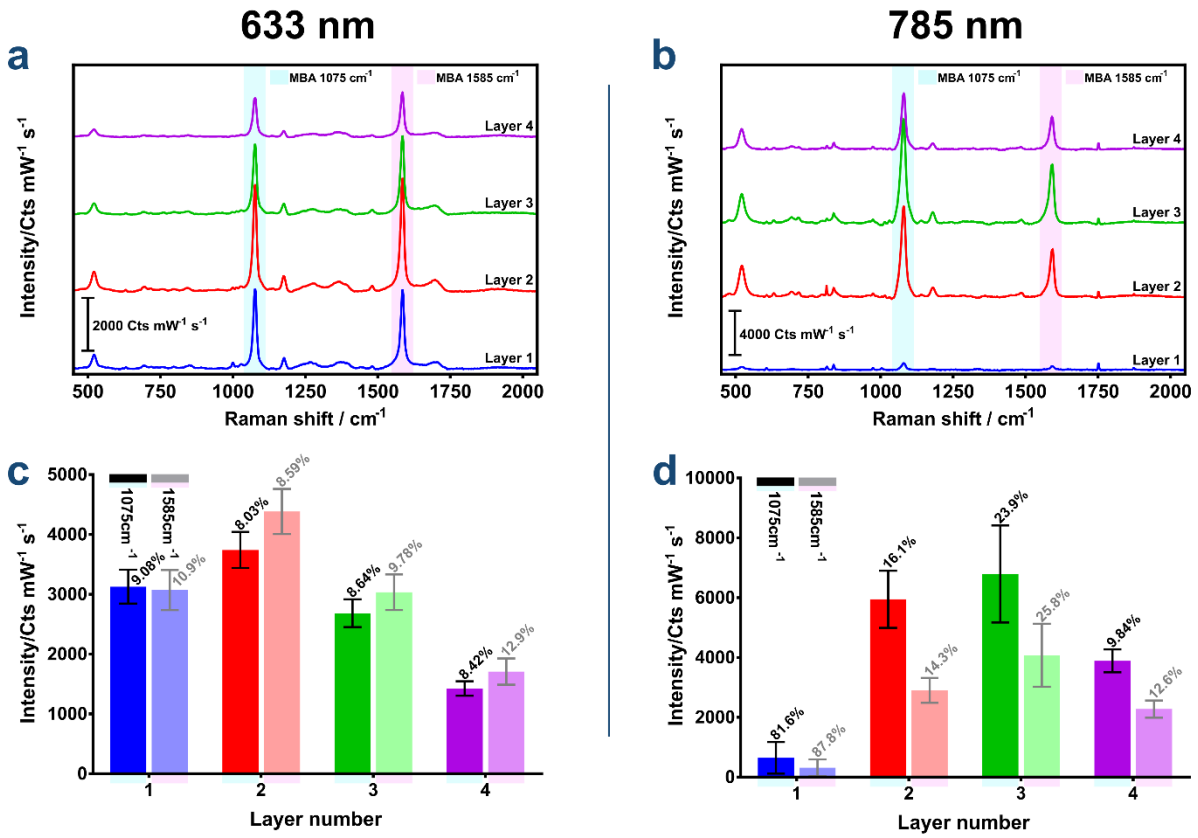

Figure 4: SERS spectra of one to four AuNP layer sensors with a (a) 633 nm and a (b) 785 nm excitation. Individual particles exposed to 10 µM 4-MBA. The intensity and variability of the two ring breathing modes of 4-MBA (1075 cm^{-1} and 1585 cm^{-1}) are shown for the 633 nm (c) and 785 nm (d) lasers. Relative standard deviation (RSD) values are indicated above error bars. For all measurements n = 10.

signals. The signals increase with the addition of subsequent two layers before they decrease again with the addition of the fourth layer. The SERS response with 785 nm excitation of the different layer sensors is along expected lines as the plasmon resonances red-shift (as shown in Figure 2d) and tune-in better with the 2 and 3 layers compared to 1 and 4 layer sensors.

The ratio between the intensity of 1075 and 1585 cm^{-1} peaks reflects the enhancement levels at the corresponding scattered wavelengths for a given number of layers (Figure 4c, d). From this perspective the sensors perform better with 633 nm excitation compared to the 785 nm excitation. Overall the 2 layer sensors gave the highest signals with the 633 nm excitation and the 3 layer sensors gave the highest signals with the 785 nm excitation. However, the reproducibility/variation (relative standard deviation (RSD)) in signals was lowest for the 2 layer sensor with 633 nm excitation. The reproducibility in signals for the 2 layer sensors was also better than a single layer sensor, likely due to higher uniformity in nanoparticle coverage achieved.

Importantly, all sensors, from one to four AuNP layers, provide highly reproducible measurements (RSD 8-12%, *n* = 10). The RSDs of the peak intensities provide a means to assess the sensor's measurement reproducibility. Differences not only reflect inconsistencies of the nanostructured material, but also systemic/handling variations. Given that the variation of AuNPs size is specified to be 8%, the obtained RSD indicates beneficial contribution from ensemble averaging.

The previous experiments identified the 2 AuNP layer assembly as being optimal, with it proving to be the most reproducible sensor when a 633 nm excitation source is used. With the 4-MBA reporter molecule the sensors are found to have a deviation of around 8% and 8.6% for the two peaks. Sensors of this conformation also provide an enhancement factor (EF) of approximately 9 x 10^5 (see S4 for Calculations). The enhancement and reproducibility with both excitation wavelengths exceeds the other layer configurations, making it the preferred construct for calibrated sensing.

Quantitative SERS sensing using internal 'calibration' standard

So far we have shown how to use layer-by-layer technology to fabricate reproducible SERS sensors that can be optimized for specific excitation wavelengths and major peaks of an analyte. In addition, the LbL approach allows the creation of multiple SERS-active zones within a composite colloid that are isolated from each other. This can be used to embed internal standards. Internal standards are of particular interest for constructing SERS substrates because they overcome effects such as fluctuating laser power, change of focus or drift within the optical alignment and even differences in the enhancement factor (EF),[40] and thereby provide a means for improved quantification.

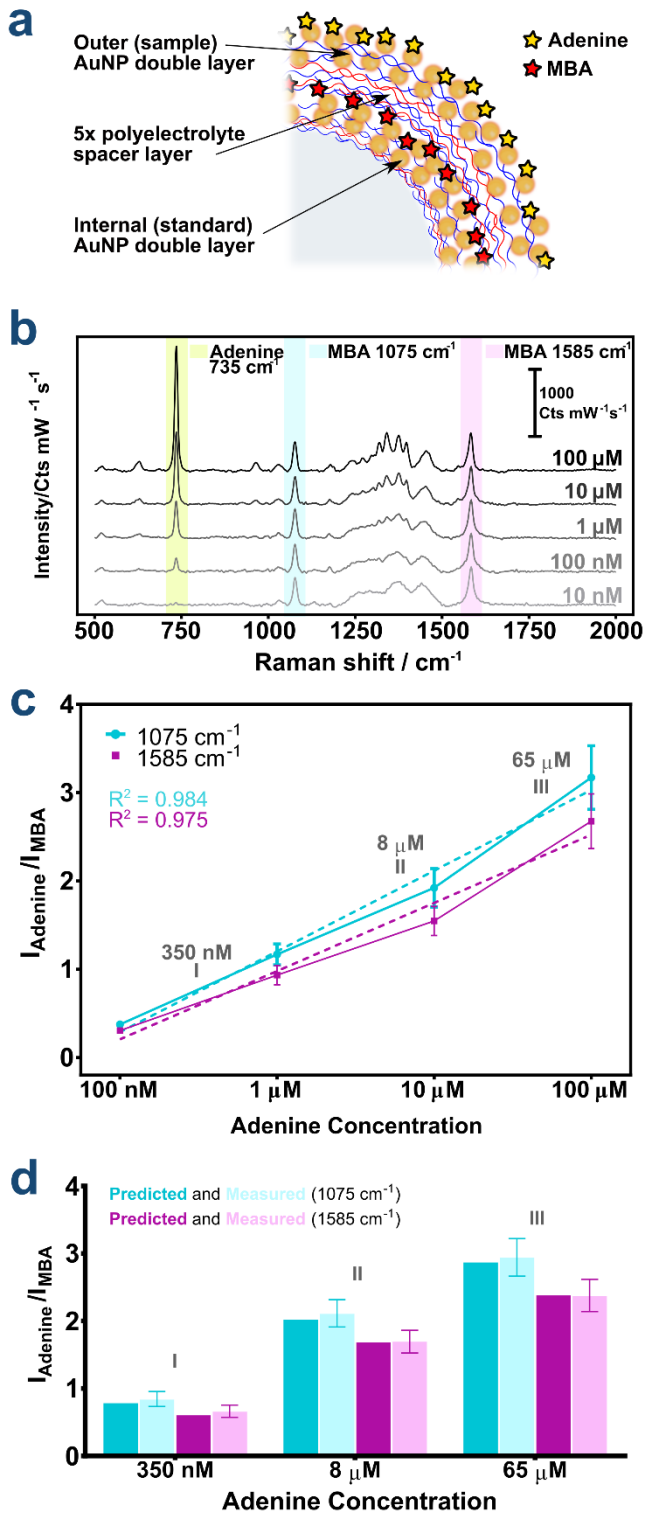

Figure 5: (a) Schematic for internal standard sensors with two distinct SERS active regions separated by polyelectrolyte spacer layers. (b) Spectra of internal standard sensors exposed to various concentrations of adenine in non-saturating conditions. The prominent ring breathing peak (735 cm^{-1}) visibly increases in line with the increase of analyte concentration. (c) Concentration calibration curves based on the 735 cm^{-1} adenine peak after normalisation to either the 1075 cm^{-1} or 1585 cm^{-1} peaks of 4-MBA. The dotted lines represent linear regressions. n = 10. (d) Predicted and measured intensities for three concentrations of adenine (based on the 735 cm^{-1} peak-intensity after 4-MBA normalization). Values within the bars denote % error between the predicted and measured mean. RSDs are detailed above error bars. n = 5.

To demonstrate the concept, SERS sensors for 633 nm excitation with an internal standard based on 4-MBA were developed to measure adenine concentrations. As noted above we found that the 2-layer sensors showed the highest and most reproducible enhancement. Therefore we chose the 2-layer configuration as the basis for developing self-calibrating sensors with an internal standard. Adenine was selected as the model analyte as it has a main ring breathing peak at ~735 cm^{-1},[41] distinct from 4-MBA peaks. 4-MBA covalently attaches to the gold via a thiol bond forming a monolayer and therefore is well suited as an internal standard. The sensors consist of three main elements (Figure 5a), the first being an internal SERS-active zone consisting of two AuNP layers that are exposed to the 'internal standard' 4-MBA SERS reporter at a saturating concentration (*i.e.* 10 µM) during assembly. The second zone is a spacer layer consisting of 5 polyelectrolyte layers $((PEI/PSS)_2PEI)$ that is used to distance and optically isolate the 'internal standard zone' from the second SERS-active zone for analyte (adenine) sensing. 5 intervening polyelectrolyte layers were optimal to maintain the integrity of the 'internal standard' SERS-active zone by optical isolation. Figure S5 shows scattering data from a sensor with two-SERS active zones separated by 5 intervening polyelectrolyte spacer layers for comparison with 2-layer and 4-layer sensor constructs obtained by consecutive deposition of layers. The scattering spectra demonstrate that the sensor with two isolated SERS-active zones (the 'internal standard' sensor) is more similar to a 2-layer sensor than a 4-layer sensor. This confirms that the two SERS active zones separated by 5 spacer layers are sufficiently decoupled. Sensors with 3 spacer layers were also investigated but proved less suitable due to the formation of a second scattering peak (Figure S5). Lack of consistent and reproducible optical isolation in these sensors resulted in larger fluctuations in peak intensities and corresponding ratios between peaks when compared to sensors with 5 spacer layers (Table S6).

Figure 5b presents spectra taken with 633 nm excitation for the internal standard sensors exposed to adenine in concentrations varying from 100 µM to 10 nM, where 10 nM was found to be the limit of detection (LOD) experimentally. From analysis of the data the limit of quantification (LOQ) is estimated to be 33 nM. The data from 100 nM onwards is used to plot a linear calibration curve (Figure 5c) by normalizing ten single particle spectra by either the 1075 cm^{-1} or 1585 cm^{-1} peaks of 4-MBA and calculating a mean of the normalized adenine 735 cm^{-1} peak. Linear regression was used to fit the SERS data from the sensors to obtain the calibration curve (Figure 5c). It shows that the dynamic range is linear over the three orders of magnitude range tested here for the sensors. In order to further establish the quantitative ability of the sensors, 'single-blinded' measurements were conducted with three adenine concentrations (65 µM, 8 µM, and 350 nM), providing an unbiased quantitative assessment. The sensors were soaked in analyte as before and 5 particles measured from each sample to determine a mean. Figure 5d shows how the measured concentrations (as given by the calibration curve) compared with actual (prepared) concentrations. The results present a high degree of accuracy with % errors ranging from 3.8% - 7.4% after normalization to the 1075 cm^{-1} peak, and 0.42% - 3.8% after normalization to the 1585 cm^{-1} peak. Thus accuracies can reach >99.5% at µM concentrations while overall they were always found >92.6%. Good precision is also

demonstrated with RSDs ranging from 9.44% - 13.7%. Whilst there is an increase in RSD versus standard 2 layer sensors, these values are markedly lower than the individual combined RSDs of the adenine peak and either of the 4-MBA peaks, showing that the internal standard provides a platform for highly quantitative measurements. It is noteworthy to mention that our approach of utilising the LbL approach for making colloidal SERS sensors with an internal standard is unique and therefore comparison with similar SERS sensors is difficult. Nevertheless, the fabrication method is elegant, inexpensive and the sensors are field deployable; where relevant data is available we can say that the quantitation ability is comparable or better than other self-calibrating (internal standard) SERS strategies including those published by us earlier.[42–44]

Conclusions

In summary, we have developed an accessible way to prepare reproducible and quantitative colloidal sensors with tunable localized surface plasmon resonances based on sequential adsorption of polyelectrolyte/AuNP layers. The high level of spatial control afforded by the LbL approach allows SERS-active zones to be isolated within sensors, enabling the incorporation of internal standards that allow accurate and reproducible analyte quantification. This simple approach offers the construction of bespoke and multi-functional sensors for diverse analytical sensing applications.

Conflicts of interest

There are no conflicts to declare.

Acknowledgements

This work was supported by the University of Southampton (Institute for Life Sciences and Department of Chemistry). SM acknowledges funding support from ERC (NanochemBioVision: 638258)

Notes and references

1 D. L. Jeanmaire and R. P. Van Duyne, *J. Electroanal. Chem. Interfacial Electrochem.*, 1977, **84**, 1–20.
2 M. G. Albrecht and J. A. Creighton, *J. Am. Chem. Soc.*, 1977, **99**, 5215–5217.
3 P. L. Stiles, J. a Dieringer, N. C. Shah and R. P. Van Duyne, *Annu. Rev. Anal. Chem. (Palo Alto. Calif).*, 2008, **1**, 601–26.
4 K. Kneipp, Y. Wang, H. Kneipp, L. T. Perelman, I. Itzkan, R. R. Dasari and M. S. Feld, *Phys. Rev. Lett.*, 1997, **78**, 1667–1670.
5 S. Nie, *Science (80-.).*, 1997, **275**, 1102–1106.
6 M. Moskovits, *Rev. Mod. Phys.*, 1985, **57**, 783–826.
7 S. Abalde-Cela, S. Carregal-Romero, J. P. Coelho and A. Guerrero-Martínez, *Adv. Colloid Interface Sci.*, 2016, **233**, 255–270.
8 M. Kahl, E. Voges, S. Kostrewa, C. Viets and W. Hill, *Sensors Actuators B Chem.*, 1998, **51**, 285–291.
9 J. Yao, A. P. Le, S. K. Gray, J. S. Moore, J. A. Rogers and R. G. Nuzzo, *Adv. Mater.*, 2010, **22**, 1102–1110.
10 J. Zhang, Y. Li, X. Zhang and B. Yang, *Adv. Mater.*, 2010, **22**, 4249–4269.
11 Z. Tian, B. Ren and D. Wu, *J. Phys. Chemsitry*, 2002, **106**, 9463–9483.
12 R. F. Aroca, R. A. Alvarez-Puebla, N. Pieczonka, S. Sanchez-Cortez and J. V. Garcia-Ramos, *Adv. Colloid Interface Sci.*, 2005, **116**, 45–61.
13 A. Shiohara, Y. Wang and L. M. Liz-marzán, *"Journal Photochem. Photobiol. C Photochem. Rev.*, 2014, **21**, 2–25.
14 R. W. Taylor, T. Lee, O. A. Scherman, R. Esteban, J. Aizpurua, F. M. Huang, J. J. Baumberg, S. Mahajan and T. E. T. Al, *ACS*, 2011, 3878–3887.
15 K. R. Ackermann, T. Henkel and J. Popp, *Chemphyschem*, 2007, **8**, 2665–70.
16 R. Gao, N. Choi, S.-I. Chang, S. H. Kang, J. M. Song, S. I. Cho, D. W. Lim and J. Choo, *Anal. Chim. Acta*, 2010, **681**, 87–91.
17 R. Gao, N. Choi, S.-I. Chang, E. K. Lee and J. Choo, *Nanoscale*, 2014, **6**, 8781–6.
18 W. W. Y. Lee, V. A. D. Silverson, C. P. Mccoy, R. F. Donnelly and S. E. J. Bell, *Anal. Chem.*, 2014, **86**, 8106–8113.
19 G. Decher, *Science (80-.).*, 1997, **277**, 1232–1237.
20 J. J. Richardson, J. Cui, M. Björnmalm, J. A. Braunger, H. Ejima and F. Caruso, *Chem. Rev.*, 2016, **116**, 14828–14867.
21 G. B. Sukhorukov, E. Donath, H. Lichtenfeld, E. Knippel, M. Knippel, A. Budde and H. Möhwald, *Colloids Surfaces A Physicochem. Eng. Asp.*, 1998, **137**, 253–266.
22 Z. Tang, Y. Wang, P. Podsiadlo and N. A. Kotov, *Adv. Mater.*, 2006, **18**, 3203–3224.
23 K. Ariga, Y. Yamauchi, G. Rydzek, Q. Ji, Y. Yonamine, K. C.-W. Wu and J. P. Hill, *Chem. Lett.*, 2014, **43**, 36–68.
24 N. A. Kotov, I. Dekany and J. H. Fendler, *J. Phys. Chem.*, 1995, **99**, 13065–13069.
25 D. S. Dos Santos, R. C. Sanfelice, R. Alvarez-Puebla, O. N. Oliveira and R. F. Aroca, *Macromol. Symp.*, 2006, **245–246**, 325–329.
26 S. Vial, I. Pastoriza-Santos, J. Pérez-Juste and L. M. Liz-Marzán, *Langmuir*, 2007, **23**, 4606–4611.
27 S. Abalde-Cela, S. Ho, B. Rodríguez-González, M. a. Correa-Duarte, R. a. Álvarez-Puebla, L. M. Liz-Marzán and N. a. Kotov, *Angew. Chemie - Int. Ed.*, 2009, **48**, 5326–5329.
28 Z. Liu, Z. Yan and L. Bai, *Appl. Surf. Sci.*, 2016, **360**, 437–441.
29 Y. Han, S. Sukhishvili, H. Du, J. Cefaloni and B. Smolinski, *J. Nanosci. Nanotechnol.*, 2008, **8**, 5791–5800.
30 J. Trevisan, P. P. Angelov, A. D. Scott, P. L. Carmichael and F. L. Martin, *Bioinformatics*, 2013, **29**, 1095–1097.
31 K. Tang and N. A. M. Besseling, *Soft Matter*, 2016, **12**, 1032–1040.
32 B. Zeeb, C. Thongkaew and J. Weiss, *J. Appl. Polym. Sci.*, 2014, **131**, 1–11.
33 A. A. Kokhanovsky and E. P. P. Zege, *J. Aerosol Sci.*, 1997, **28**, 1–21.
34 S. Bakhti, A. V. Tishchenko, X. Zambrana-Puyalto, N. Bonod, S. D. Dhuey, P. J. Schuck, S. Cabrini, S. Alayoglu and N. Destouches, *Sci. Rep.*, 2016, **6**, 1–12.
35 S. J. Barrow, A. M. Funston, D. E. Gómez, T. J. Davis and P. Mulvaney, *Nano Lett.*, 2011, **11**, 4180–4187.

36 L. Gunnarsson, T. Rindzevicius, J. Prikulis, B. Kasemo, M. Käll, S. Zou and G. C. Schatz, *J. Phys. Chem. B*, 2005, **109**, 1079–1087.

37 P. K. Jain, S. Eustis and M. A. El-Sayed, *J. Phys. Chem. B*, 2006, **110**, 18243–18253.

38 S. Schlücker, *Chemphyschem*, 2009, **10**, 1344–54.

39 A. Michota and J. Bukowska, *J. Raman Spectrosc.*, 2003, **34**, 21–25.

40 S. E. J. Bell and N. M. S. Sirimuthu, *Chem. Soc. Rev.*, 2008, **37**, 1012.

41 J. De Gelder, K. De Gussem, P. Vandenableele and L. Moens, *J. Raman Spectrosc.*, 2007, **38**, 1133–1147.

42 W. Shen, X. Lin, C. Jiang, C. Li, H. Lin, J. Huang, S. Wang, G. Liu, X. Yan, Q. Zhong and B. Ren, *Angew. Chemie - Int. Ed.*, 2015, **54**, 7308–7312.

43 A. Lorén, J. Engelbrektsson, C. Eliasson, M. Josefson, J. Abrahamsson, M. Johansson and K. Abrahamsson, *Anal. Chem.*, 2004, **76**, 7391–7395.

44 S. Kasera, F. Biedermann, J. J. Baumberg, O. A. Scherman and S. Mahajan, *Nano Lett.*, 2012, **12**, 5924–5928.